Supporting Information for

Effects of Halogenation in B←N Embedded Polymer Acceptors on Performance of All-polymer Solar Cells

Huifeng Meng,[†, #, ¶] *Yongchun Li,*[†, #, ¶] *Bo Pang,*[†] *Yuqing Li,*[†, #] *Ying Xiang,*[†] *Liang Guo,*[†] *Xuemei Li,*[*, ‡] *Chuanlang Zhan,*[*, #] *Jianhua Huang,*[*, †]

[†] College of Materials Science and Engineering, Huaqiao University, Xiamen, 361021, P. R. China.
[‡] School of Chemistry & Chemical Engineering, Linyi University, Linyi 276000, China.
[#] CAS key Laboratory of Photochemistry, Institute of Chemistry, Chinese Academy of Sciences, Beijing 100190 China

Corresponding Authors
E-mail: huangjianhua@hqu.edu.cn (J.H.); xuemei_li@yeah.net (X. L); clzhan@iccas.ac.cn (C.Z);

Contents

1 Experimental Section

1.1 Materials and Instruments

All reagents and reactants were purchased commercially and used directly without further purification unless otherwise stated. Tetrahydrofuran and toluene were distilled freshly from sodium benzophenone ketyl under nitrogen before use. Dichloromethane, chloroform, and triethylamine were dried over calcium hydride, distilled under N_2 atomsphere, and stored over molecular sieves (3 Å). Molecular sieves (3 Å) were purchased from Energy Chemical and dried at 120 ºC under vacuum for 24 h before use. PBDB-T, BDT-Sn, BDT-F-Sn, and BDT-Cl-Sn were purchased from Solarmer. BNIDT-Br was synthesized according to our previous work.[1] The ^{1}H NMR spectra were measured on a Bruker AVANCE 500 MHz spectrometer using tetramethylsilane (TMS; δ = 0 ppm) as an internal standard. Temperature-dependent UV-vis absorption spectra of polymer solutions at various temperatures were collected on the Hitachi UH4150. The electrochemical measurements were carried out in a deoxygenated solution of tetra-n-butylammonium hexafluorophosphate (Bu_4NBF_6, 0.1 M) in acetonitrile, with a computer-controlled Zennium electrochemical workstation. A glassy carbon electrode, a Pt wire, and saturated calomel electrode (SCE) electrode were used as the working, counter, and reference electrodes, respectively. Ferrocene/ferrocenium (Fc/Fc+) redox pair was used as the internal standard. The polymers were deposited on the glassy carbon electrode for measurements. The scanning rate was 100 mV/s. The molecular weight of the polymers was measured by gel permeation chromatograph (GPC, Waterwate) in THF using polystyrene as a standard. Thermogravimetric (TGA) was recorded on DTG-50H at a heating rate of 10 ºC/min under air condition. Atomic force microscope (AFM) was performed on a Nanoscope V AFM (Digital Instruments) in tapping mode. TEM tests were performed on a JEM-2011F operated at 200 kV. TEM samples were obtained by transferring the floated blend films from the water onto the Cu grid. All the blend films were fabricated under the optimal conditions.

1.2 Gaussian Calculations

Density functional theory (DFT) calculations were performed using the Gaussian 09 program with the B3LYP exchange-correlation functional.[2-4] All-electron double-ξ valence basis sets with polarization functions (6-31G (d, p)) are used for all atoms. Geometry optimizations were performed with full relaxation of all atoms. All alkyl chains were omitted or educed to methyl groups for avoiding computational load. For each molecule, various conformations with different dihedral angles were optimized, and the data for the one with the lowest energy are reported. HOMO and LUMO orbitals were deduced from cub files on Gaussian view. The electrostatic potential surface (EPS) maps were exported from fchk files on Gaussian view linked to Gaussian 09 program.

1.3 Fabrication and Tests of Photovoltaic Devices

The all polymer solar cells were fabricated in the conventional structure of ITO/PEDOT: PSS/active layer/PDINO/Al. The commercially purchased ITO substrates were scrubbed with detergent and then sonicated with deionized water, acetone, isopropanol subsequently, and dried over night prior to use. UV-O_3 treatment was applied to the cleaned ITO substrates for 30 min. PEDOT: PSS ((Heraeus Clevios P VP AI 4083) was spin-coated on the ITO at 4000 rpm for 30 s and then dried at 150 ºC for 15 min in air. PBDB-T: polymer acceptor blends were dissolved in chloroform and stirred overnight on a hotplate at 55 ºC in a nitrogen-filled glove box. The active solutions were spin-coated onto the ITO/PEDOT: PSS substrates at different rotation speed for 40 s followed by thermal annealing at different temperature. A thin PDINO was coated on the active layer followed by the deposition of Al (ca. 800 Å) (evaporated under 5×10^{-5} Pa through a shadow mask). The optimal active layer thickness measured by a Bruker Dektak XT stylus profilometer was ca. 100 nm. The current density-voltage (*J-V*) curves were measured using a Keithley 2400 Source Meter in air under AM 1.5G (100 mW•cm^{-2}) using a Newport solar simulator. The light intensity was calibrated using a standard Si diode (with KG5 filter, purchased

from PV Measurement to bring spectral mismatch to unity). External quantum efficiencies (EQEs) were measured using an Enlitech QE-R EQE system equipped with a standard Si diode. Monochromatic light was generated from a Newport 300W lamp source.

1.4 Space-Charge Limited Current (SCLC) Tests

The electron-only devices were fabricated with a configuration of ITO/titanium (diisopropoxide) bis(2,4-pentanedionate) (TIPD)/active layer/PDINO/Al and hole-only devices were configured with ITO/PEDOT:PSS/active layer/ Au. The TIPD buffer layer was prepared by spin-coating a 3.5 wt % TIPD isopropanol solution onto the pre-cleaned ITO substrate and then baked at 150 °C for 10 min to convert TIPD into TOPD.[5] Subsequently, the blend was spin-coated on it under the same condition as preparation of the optimal solar cell. The Al layer was thermally deposited on the top of the blend in vacuum at a speed of 1 Å/ s. The electron and hole mobilities were extracted by fitting the current density-voltage curves using the Mott-Gurney law,[5,6]

$$J_{SCL} = \frac{9\varepsilon\varepsilon_0\mu V^2}{8L^3} \quad (1)$$

where ε is the dielectric constant of the organic component, ε_0 is the permittivity of the vacuum (8.85419×10^{-12} $CV^{-1}m^{-1}$), μ is the zero-field mobility, J_{SCL} is the current density, L is the thickness of the active layer, and $V = V_{app} - V_{bi}$, here V_{app} is the applied potential, and V_{bi} the built-in potential which results from the difference in the work function values of the cathode. From the plot of $J^{1/2}$ versus V, the hole and electron mobilities can be deduced.

2 Supporting Tables and Figures

2.1 Supporting Tables

Table S1. Rotation speed optimization of PBDB-T: BN-BDT-based devices.

Condition	Rotation speed (rpm)	V_{oc} (V)	J_{sc} (mA/cm^2)	FF (%)	$PCE_{max/avg}$ (%)
Solvent: CF 16 mg/mL D: A = 3:2	1500	0.99	2.78	30.48	0.83 (0.71) [a]
	2000	0.98	2.94	30.12	0.87 (0.79) [a]
	2500	0.99	3.70	29.58	1.08 (0.97) [a]
	3000	0.99	3.47	30.04	1.03 (0.96) [a]
	3500	1.00	3.29	30.91	1.02 (0.95) [a]

[a] Statistic efficiencies averaged from 10 cells.

Table S2. Thermal annelaing optimization of PBDB-T: BN-BDT-based devices.

Condition	Annealing (ºC)	V_{oc} (V)	J_{sc} (mA/cm^2)	FF (%)	$PCE_{max/avg}$ (%)
Solvent: CF 16 mg/mL D: A = 3:2 2500 rpm	100	0.82	2.20	29.05	0.53 (0.52) [a]
	110	0.95	2.67	30.00	0.76 (0.72) [a]
	120	0.95	2.72	30.39	0.79 (0.76) [a]
	130	0.94	2.49	31.38	0.73 (0.72) [a]
	140	0.93	2.79	31.19	0.81 (0.79) [a]
	150	0.93	2.96	31.68	0.87 (0.83) [a]
	160	0.93	2.86	32.48	0.86 (0.83) [a]

[a] Statistic efficiencies averaged from 10 cells.

Table S3. Active layer concentration optimization of PBDB-T: BN-BDT-based devices.

Condition	Concentration (mg/mL)	V_{oc} (V)	J_{sc} (mA/cm^2)	FF (%)	$PCE_{max/avg}$ (%)
Solvent: CF Thermal annealing: 150 ºC, 10 min D: A = 3:2 2500 rpm	8	0.98	2.66	40.09	1.04 (0.99) [a]
	10	0.96	4.31	34.73	1.44 (1.32) [a]
	12	0.95	3.43	34.93	1.14 (1.02) [a]
	14	0.94	3.18	33.26	0.99 (0.80) [a]

[a] Statistic efficiencies averaged from 10 cells.

Table S4. The optimized condition for BN-BDT

Condition	V_{oc} (V)	J_{sc} (mA/cm^2)	FF (%)	$PCE_{max/avg}$ (%)
Solvent: CF Thermal annealing: 150 ºC, 10 min D: A = 3:2 2500 rpm 10 mg/mL	0.98	4.26	38.25	1.60 (1.54) [a]

[a] Statistic efficiencies averaged from 10 cells.

Table S5. Rotation speed optimization of PBDB-T: BN-BDT-F-based devices.

Condition	Rotation speed (rpm)	V_{oc} (V)	J_{sc} (mA/cm^2)	FF (%)	$PCE_{max/avg}$ (%)
Solvent: CF 16 mg/mL D: A = 3:2	1500	0.97	4.72	28.47	1.31 (1.21) [a]
	2000	0.99	5.69	29.37	1.65 (1.52) [a]
	2500	0.99	6.15	30.51	1.85 (1.72) [a]
	3000	1.00	7.25	31.86	2.31 (2.03) [a]
	3500	1.00	7.13	31.94	2.73 (2.17) [a]
	4000	1.00	6.43	31.82	2.08 (2.00) [a]
	4500	1.00	6.58	32.04	2.14 (2.05) [a]

[a] Statistic efficiencies averaged from 10 cells.

Table S6. Thermal annelaing optimization of PBDB-T: BN-BDT-F-based devices.

Condition	Annealing (ºC)	V_{oc} (V)	J_{sc} (mA/cm^2)	FF (%)	$PCE_{max/avg}$ (%)
Solvent: CF 16 mg/mL D: A = 3:2 3000 rpm	100	1.00	7.56	33.73	2.58 (2.53) [a]
	110	1.00	7.60	33.40	2.58 (2.54) [a]
	120	1.00	6.93	35.20	2.46 (2.41) [a]
	130	1.00	6.87	35.56	2.47 (2.42) [a]
	140	1.00	7.31	36.04	2.64 (2.59) [a]
	150	0.99	7.46	35.75	2.78 (2.63) [a]
	160	1.00	7.19	37.84	2.74 (2.68) [a]

[a] Statistic efficiencies averaged from 10 cells.

Table S7. D/A ratio optimization of PBDB-T: BN-BDT-F-based devices.

Condition	D:A	V_{oc} (V)	J_{sc} (mA/cm^2)	FF (%)	$PCE_{max/avg}$ (%)
Solvent: CF 16 mg/mL Thermal annealing: 150 ºC, 10 min 3000 rpm 0.6%DIO	2:1	0.96	6.56	36.31	2.27 (2.19) [a]
	3:2	0.97	7.64	38.51	2.86 (2.63) [a]
	1:1	0.98	6.28	38.25	2.36 (2.32) [a]
	2:3	1.00	5.95	38.13	2.27 (2.19) [a]
	1:2	1.00	5.16	36.42	1.88 (1.82) [a]

[a] Statistic efficiencies averaged from 10 cells.

Table S8. Active layer concentration optimization of PBDB-T: BN-BDT-F-based devices.

Condition	Concentration (mg/mL)	V_{oc} (V)	J_{sc} (mA/cm^2)	FF (%)	$PCE_{max/avg}$ (%)
Solvent: CF Thermal annealing: 150 ºC, 10 min D: A = 3:2 3000 rpm	5	0.95	6.47	42.16	2.58 (2.32) [a]
	8	0.97	8.33	43.23	3.47 (3.29) [a]
	10	0.96	8.84	43.79	3.71 (3.66) [a]
	12	0.95	8.22	34.16	2.67 (2.55) [a]

[a] Statistic efficiencies averaged from 10 cells.

Table S9. DIO content optimization of PBDB-T: BN-BDT-F-based devices.

Condition	DIO% (v/v)	V_{oc} (V)	J_{sc} (mA/cm^2)	FF (%)	$PCE_{max/avg}$ (%)
Solvent: CF 10 mg/mL Thermal annealing: 150 ºC, 10 min D: A = 3:2 3000 rpm	0	0.96	8.84	43.79	3.71 (3.66) [a]
	0.5	0.97	4.04	37.03	1.45 (1.43) [a]
	1	0.96	2.86	33.42	0.92 (0.90) [a]
	2	0.98	3.13	36.69	1.13 (1.08) [a]

[a] Statistic efficiencies averaged from 10 cells.

Table S10. D/A ratio optimization of PBDB-T:BN-BDT-Cl-based devices.

Condition	D:A	V_{oc} (V)	J_{sc} (mA/cm^2)	FF (%)	$PCE_{max/avg}$ (%)
Solvent: CF 16 mg/mL Thermal annealing: 150 ºC, 10 min 3000 rpm	2:1	0.95	8.49	35.22	2.85 (2.80) [a]
	3:2	0.97	8.70	39.24	3.31 (3.12) [a]
	1:1	0.98	7.94	40.00	3.12 (2.98) [a]
	2:3	0.98	6.70	41.13	2.69 (2.61) [a]
	1:2	0.99	5.82	40.48	2.34 (2.27) [a]

[a] Statistic efficiencies averaged from 10 cells.

Table S11. Active layer concentration optimization of PBDB-T:BN-BDT-Cl-based devices.

Condition	Concentration (mg/mL)	V_{oc} (V)	J_{sc} (mA/cm^2)	FF (%)	$PCE_{max/avg}$ (%)
Solvent: CF Thermal annealing: 150 ºC, 10 min D: A = 3:2 3000 rpm	6	0.94	4.10	49.59	1.92 (1.73) [a]
	8	0.96	6.31	46.07	2.79 (2.66) [a]
	10	0.96	9.37	46.80	4.23 (4.10) [a]
	12	0.95	9.13	38.38	3.34 (3.27) [a]

[a] Statistic efficiencies averaged from 10 cells.

Table S12. DIO content optimization of PBDB-T:BN-BDT-Cl-based devices..

Condition	DIO% (v/v)	V_{oc} (V)	J_{sc} (mA/cm^2)	FF (%)	$PCE_{max/avg}$ (%)
Solvent: CF 10 mg/mL Thermal annealing: 150 ºC, 10 min D: A = 3:2 3000 rpm	0	0.96	9.37	46.80	4.23 (3.97) [a]
	0.1	0.96	8.58	44.38	3.66 (3.58) [a]
	0.3	0.98	8.52	44.77	3.73 (3.59) [a]
	0.5	0.96	8.35	42.37	3.40 (3.25) [a]

[a] Statistic efficiencies averaged from 10 cells.

2.2 Supporting Figures

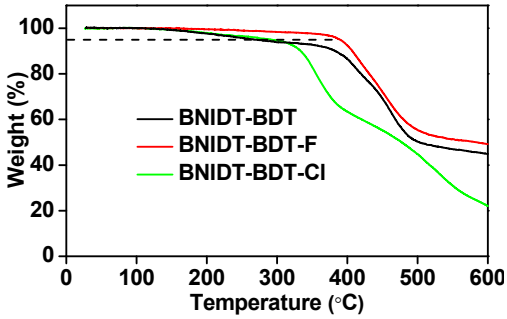

Figure S1. TGA curves of BN-BDT, BN-BDT-F, and BN-BDT-Cl.

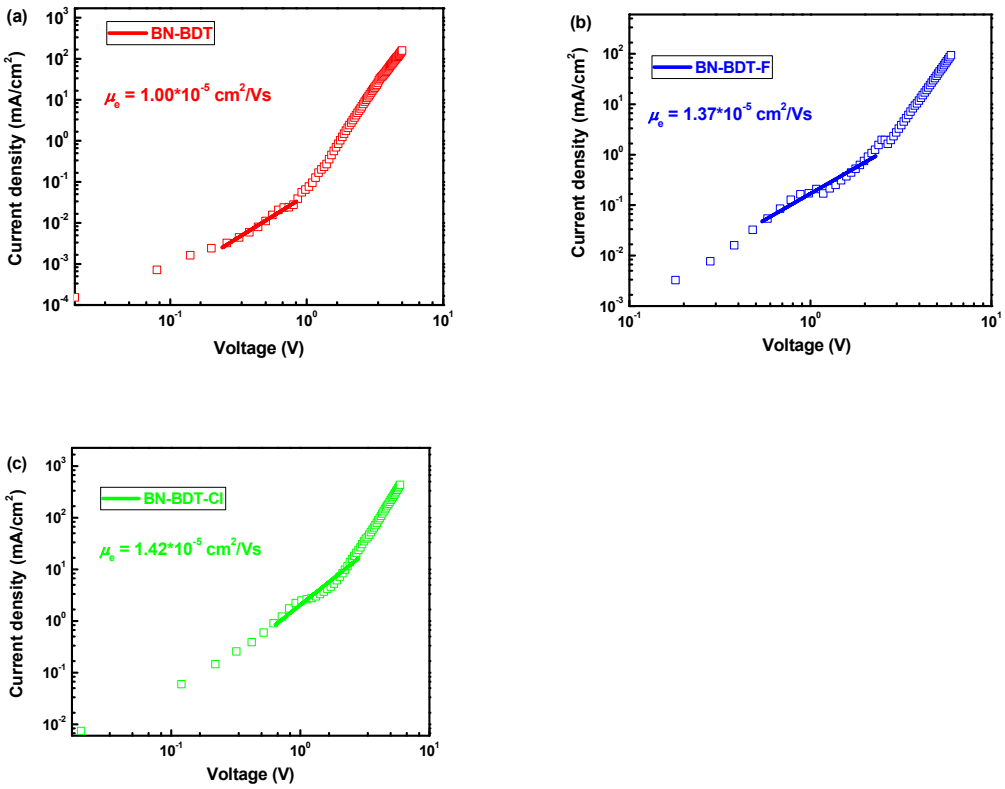

Figure S2. *J-V* plots tested by SCLC methods for electron-only devices based on BN-BDT (a), BN-BDT-F (b), and BN-BDT-Cl (c).

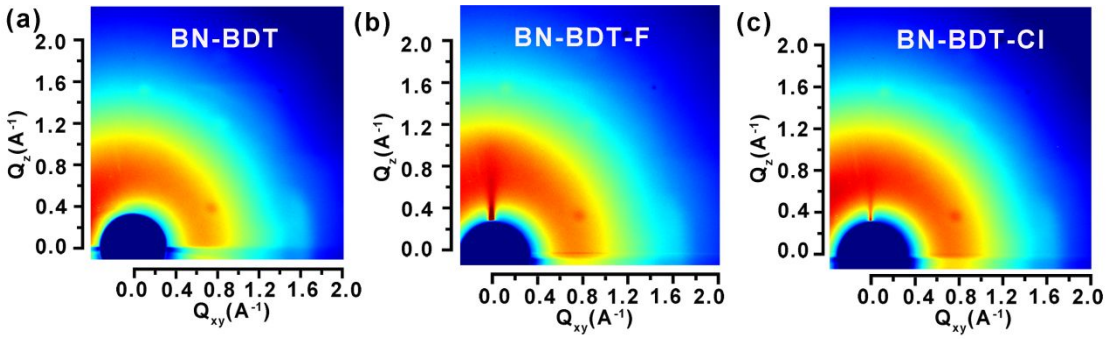

Figure S3. GIWAXS patterns of BN-BDT (a), BN-BDT-F (b), and BN-BDT-Cl (c).

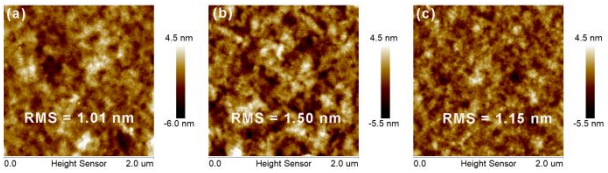

Figure S4. AFM height images of BN-BDT (a), BN-BDT-F (b), and BN-BDT-Cl (c).

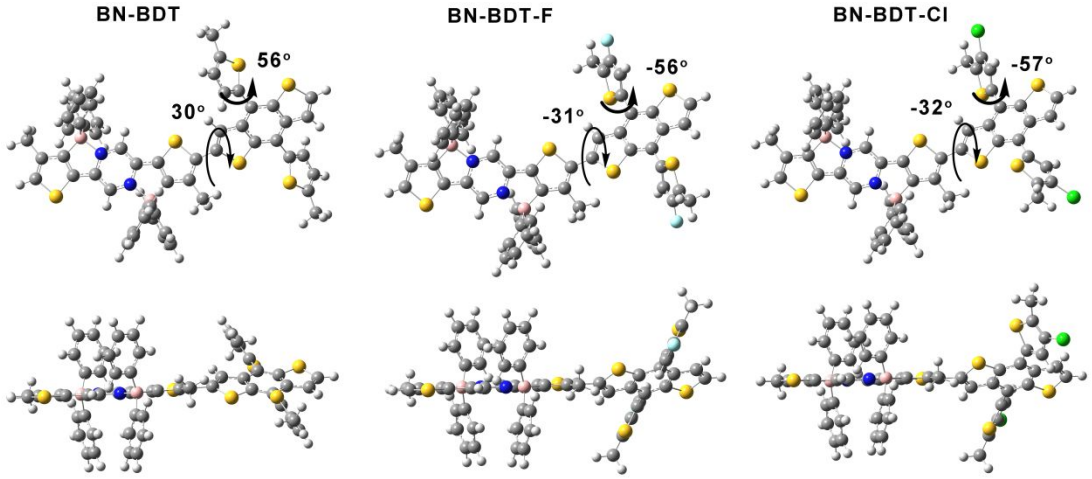

Figure S5. Optimized conformations of repeating units of BN-BDT, BN-BDT-F, and BN-BDT-Cl.

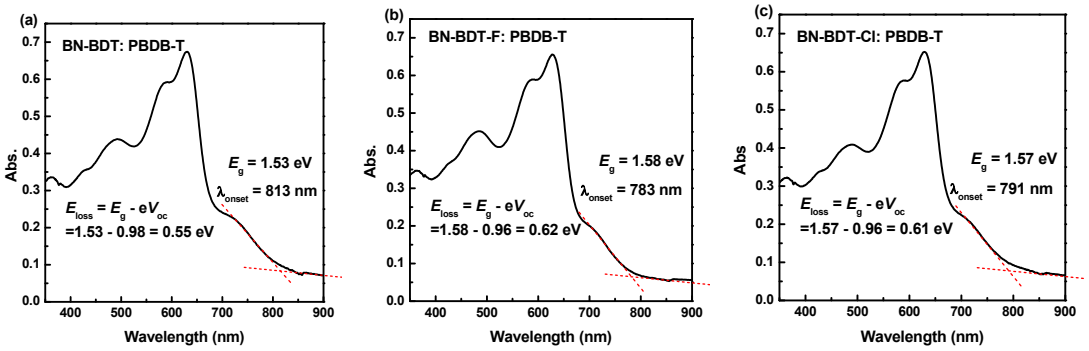

Figure S6. Absorption spectra of blend films and calculations of E_{loss} of the three devices based on BN-BDT (a), BN-BDT-F (b), and BN-BDT-Cl (c).

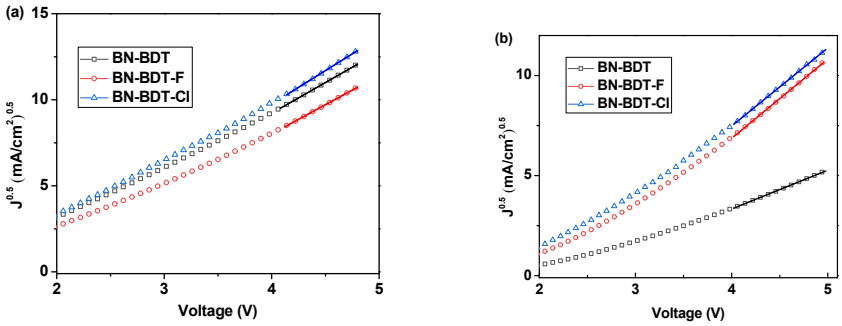

Figure S7. *J-V* plots tested by SCLC methods for electron hole (a) and electron (b)-only devices based on BN-BDT, BN-BDT-F, and BN-BDT-Cl.

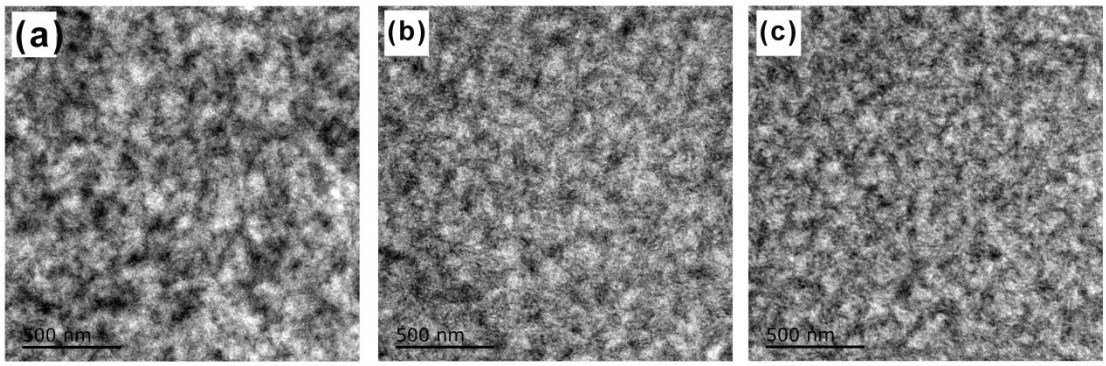

Figure S8. TEM images of PBDB-T: BN-BDT (a), PBDB-T: BN-BDT-F (b), and PBDB-T: BN-BDT-Cl (c) blend films.

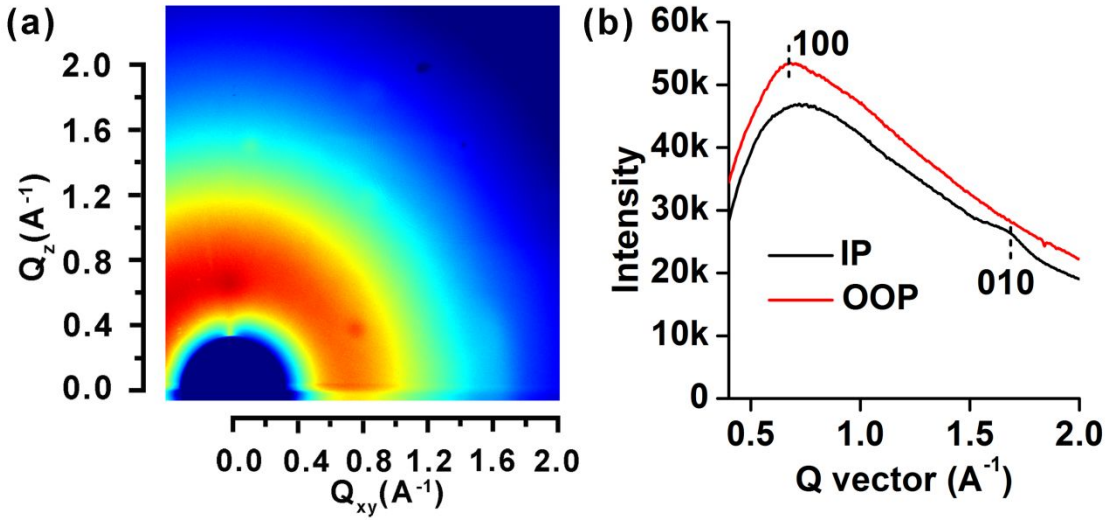

Figure S9. GIWAXS patterns of PBDB-T (a) and the line-cut profiles in the IP and OOP directions (b).

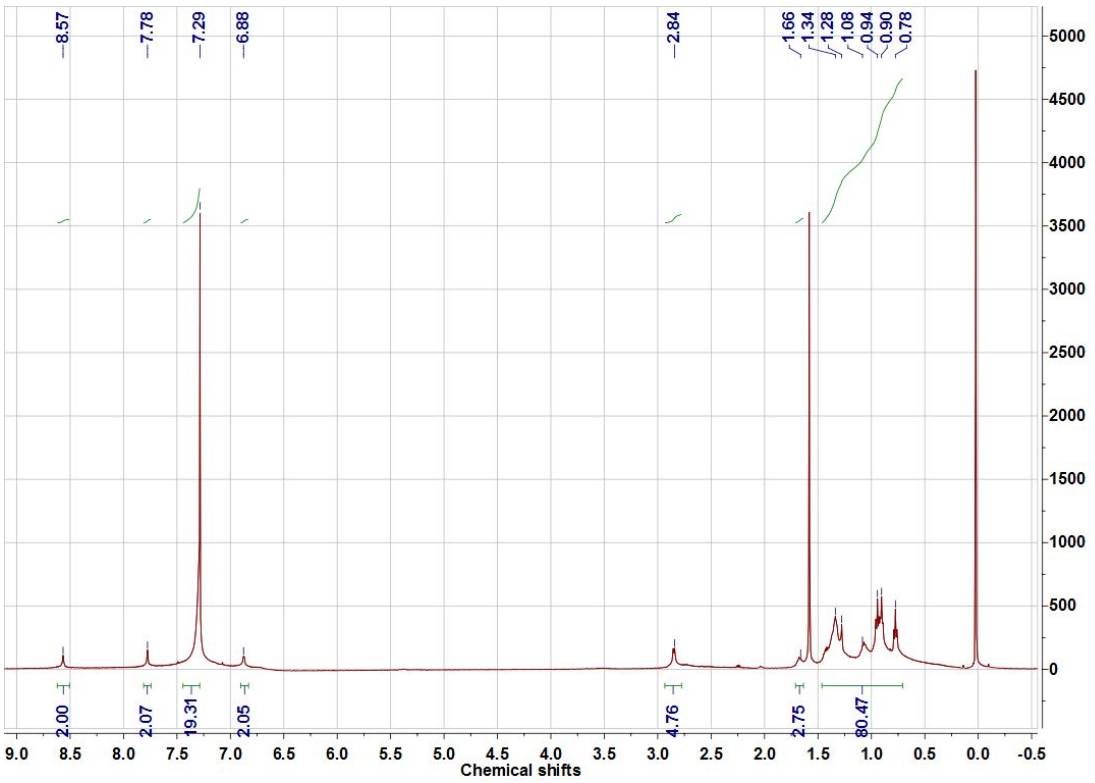

Figure S10. ^{1}H NMR spectra of BN-BDT

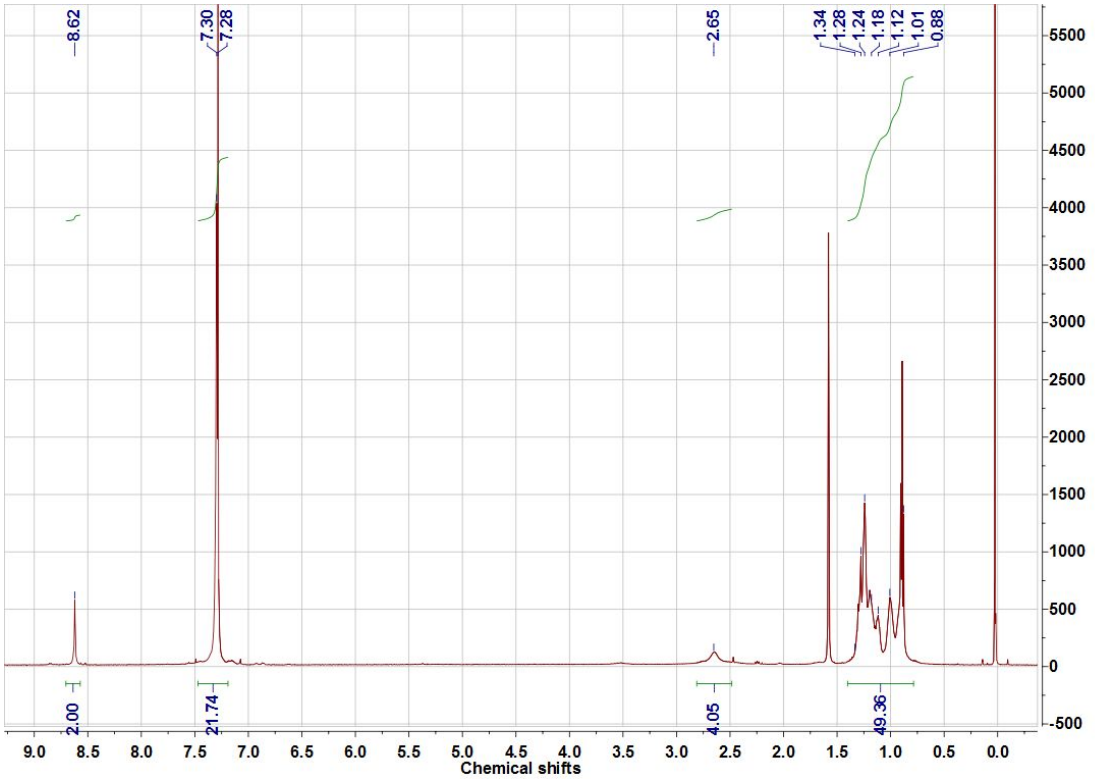

Figure S11. ^{1}H NMR spectra of BN-BDT-F

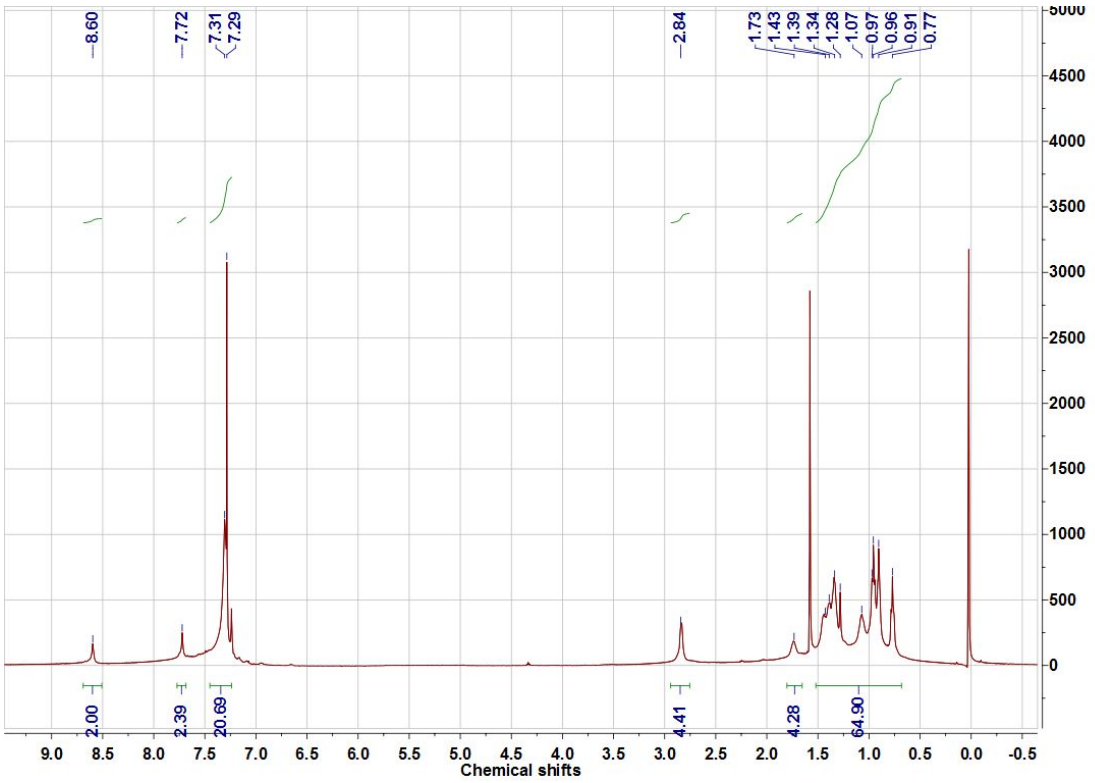

Figure S12. ^{1}H NMR spectra of BN-BDT-Cl

3 References

[1] Li, Y.; Meng, H.; Liu, T.; Xiao, Y.; Tang, Z.; Pang, B.; Li, Y.; Xiang, Y.; Zhang, G.; Lu, X.; Yu, G.; Yan, H.; Zhan, C.; Huang, J.; Yao, J. 8.78% Efficient All-Polymer Solar Cells Enabled by Polymer Acceptors Based on a B ← N Embedded Electron-Deficient Unit. *Adv. Mater*. **2019**, *31*, 1904585.

[2] Frisch, M. J.; Trucks, G. W.; Schlegel, H. B.; Scuseria, G. E.; Robb, M. A.; Cheeseman, J. R.; Montgomery Jr., J. A.; Vreven, T.; Kudin, K. N.; Burant, J. C.; Millam, J. M.; Iyengar, S. S.; Tomasi, J.; Barone, V.; Mennucci, B.; Cossi, M.; Scalmani, G.; Rega, N.; Petersson, G. A.; Nakatsuji, H.; Hada, M.; Ehara, M.; Toyota, K.; Fukuda, R.; Hasegawa, J.; Ishida, M.; Nakajima, T.; Honda, Y.; Kitao, O.; Nakai, H.; Klene, M.; Li, X.; Knox, J. E.; Hratchian, H. P.; Cross, J. B.; Bakken, V.; Adamo, C.; Jaramillo, J.; Gomperts, R.; Stratmann, R. E.; Yazyev, O.; Austin, A. J.; Cammi, R.; Pomelli, C.; Ochterski, J. W.; Ayala, P. Y.; Morokuma, K.; Voth, G. A.; Salvador, P.; Dannenberg, J. J.; Zakrzewski, V. G.; Dapprich, S.; Daniels, A. D.; Strain, M. C.; Farkas, O.; Malick, D. K.; Rabuck, A. D.; Raghavachari, K.; Foresman, J. B.; Ortiz, J. V.; Cui, Q.; Baboul, A. G.; Clifford, S.; Cioslowski, J.; Stefanov, B. B.; Liu, G.;

Liashenko, A.; Piskorz, P.; Komaromi, I.; Martin, R. L.; Fox, D. J.; Keith, T.; Al-Laham, M. A.; Peng, C. Y.; Nanayakkara, A.; Challacombe, M.; Gill, P. M. W.; Johnson, B.; Chen, W.; Wong, M. W.; Gonzalez, C.; Pople, J. A. Gaussian 09 (Gaussian, Inc., Wallingford CT, 2009).

[3] Becke, A. D. Density-Functional Exchange-Energy Approximation with Correct Asymptotic Behavior. *Phys. Rev. A* **1988**, *38*, 3098-3100.

[4] Lee, C.; Yang, W.; Parr, R. G. Development of the Colle-Salvetti Correlation-Energy Formula into a Functional of the Electron Density. *Phys. Rev. B* **1988**, *37*, 785-789.

[5] Malliaras, G. G.; Salem, J. R.; Brock, P. J.; Scott, C. Electrical Characteristics and Efficiency of Single-Layer Organic Light-Emitting Diodes. *Phys. Rev. B*, **1998**, *58*, 13411-13414.

[6] Chu, T.-Y.; Song, O.-K. Hole Mobility of N,N '-Bis(Naphthalen-1-Yl)-N,N '-Bis(Phenyl) Benzidine Investigated by Using Space-Charge-Limited Currents. *Appl. Phys. Lett.*, **2007**, *90*, 203512.